Available online at www.sciencedirect.com
SCIENCE DIRECT®
Biomaterials 27 (2006) 302–314
Biomaterials
www.elsevier.com/locate/biomaterials

A new in vivo screening model for posterior spinal bone formation: Comparison of ten calcium phosphate ceramic material treatments

Clayton E. Wilson[a,*], Moyo C. Kruyt[a], Joost D. de Bruijn[b,c], Clemens A. van Blitterswijk[c], F. Cumhur Oner[a], Abraham J. Verbout[a], Wouter J.A. Dhert[a]

[a]*Department of Orthopaedics, G05.228, University Medical Center, P.O. Box 85500, NL 3508 GA, Utrecht, The Netherlands*
[b]*Queen Mary, University of London, Mile End Road, London E1 4NS, UK*
[c]*Institute for Biomedical Technology, University of Twente, P.O. Box 217, 7500 AE Enschede, The Netherlands*

Received 29 June 2005; accepted 30 June 2005
Available online 18 August 2005

Abstract

This study presents a new screening model for evaluating the influence of multiple conditions on the initial process of bone formation in the posterior lumbar spine of a large animal. This model uses cages designed for placement on the decorticated transverse process of the goat lumbar spine. Five conduction channels per cage, each be defined by a different material treatment, are open to both the underlying bone and overlying soft tissue. The model was validated in ten adult Dutch milk goats, with each animal implanted with two cages containing a total of ten calcium phosphate material treatments according to a randomized complete block design. The ten calcium phosphate ceramic materials were created through a combination of material chemistry (BCP, TCP, HA), sintering temperature (low, medium, high), calcination and surface roughness treatments. To monitor the bone formation over time, fluorochrome markers were administered at 3, 5 and 7 weeks and the animals were sacrificed at 9 weeks after implantation. Bone formation in the conduction channels was investigated by histology and histomorphometry of non-decalcified sections using traditional light and epifluorescent microscopy. According to both observed and measured bone formation parameters, materials were ranked in order of increasing magnitude as follows: low sintering temperature BCP (rough and smooth) ≈ medium sintering temperature BCP ≈ TCP > calcined low sintering temperature HA > non-calcined low sintering temperature HA > high sintering temperature BCP (rough and smooth) > high sintering temperature HA (calcined and non-calcined). These results agree closely with those obtained in previous studies of osteoconduction and bioactivity of ceramics thereby validating the screening model presented in this study.

Keywords: Animal model; Bioactivity; Calcium phosphate; Osteoconduction; Osteogenesis

1. Introduction

Since the first investigations by Albee [1] nearly a century ago, posterior spinal fusion has become a commonly performed procedure for many orthopaedic and neurosurgical indications. The autologous bone graft is the golden standard for achieving a bony bridge between transverse processes. Despite the success of autologous grafts, bone harvest requires an extra operative procedure which incurs additional costs and carries inherent risks, such as donor site morbidity [2,3]. Therefore, substitutes for the autograft are actively being investigated. Synthetic biomaterials, such as calcium phosphate ceramics, are attractive as bone grafts substitutes due to their unlimited supply and ease of sterilization and storage. The osteoconductive nature of calcium phosphate ceramics has been well established [4–6]. Commercially available ceramic bone graft substitutes are currently utilized in posterior spinal fusion primarily as bone graft extenders [7]. These materials

*Corresponding author. Tel.: +31 30 2506971; fax: +31 30 2510638.
E-mail addresses: c.e.wilson@chir.azu.nl, c.e.wilson@tnw.utwente.nl (C.E. Wilson).

0142-9612/$ - see front matter © 2005 Elsevier Ltd. All rights reserved.
doi:10.1016/j.biomaterials.2005.06.041

have also been validated for use as bone graft substitutes for instrumented posterior spinal fusion in children and young adults [8–10]. Emerging technologies for spinal fusion, including bone inducing growth factors such as bone morphogenic proteins (BMP) and cell-based bone tissue engineering, are also utilizing porous calcium phosphate ceramics as carriers and/or scaffolds [11–13]. Furthermore, the recent identification of certain calcium phosphate materials with the inherent ability to induce bone formation is also of great potential for spinal fusion applications [14,15]. This increasing interest necessitates a relevant and efficient model, preferably in a large animal, for screening materials and conditions to support the more rapid development and optimization activities. Numerous posterior spinal fusion models have been described [16,17], however, these models are typically functional in nature, i.e. they aim to create a functional fusion of one or more spinal levels, and utilize porous granules of material. While these types of models are essential for evaluating new treatments, they are inefficient for the screening of multiple parameters. Additionally, it is difficult to ascertain how and why materials and treatments behave differently using the traditional functional models.

The purpose of the current study was to introduce and validate a new screening model for the simultaneous evaluation of multiple conditions on the initial process of bone formation. This model was inspired by the well-established multi-channel cage model of Spivak et al. [18] for evaluating intramedullary bone formation in the dog, but adapted for use on the transverse processes of the goat lumbar spine. The cages for this study were designed to hold five material conditions each. In the current study, two cages were implanted in each animal allowing ten material conditions to be evaluated. The ten material conditions examined included differences in material phases, sintering temperatures, surface roughness and calcination treatments.

2. Materials and methods

2.1. Experimental design

A total of 10 adult Dutch milk goats were used following approval of the institutional animal care committee. Two spinal cages containing a total of ten bone conduction channels (five per cage), each of a different ceramic material condition, were implanted bilaterally on the transverse process of the L4 vertebrae of each goat according to a randomized complete block design. To monitor the bone formation over time, fluorochrome markers were administered at 3, 5 and 7 weeks and the animals were sacrificed at 9 weeks after implantation. Bone formation into conduction channels was investigated by histology and histomorphometry of non-decalcified sections using epifluorescent and light microscopy.

2.2. Cages

Polyacetal cages were designed for fixation to the transverse process of the goat lumbar spine. Each cage consisted of two side walls, two end pieces, four stainless steel machine screws for cage assembly and two self-tapping bone screws to attach the cage to the transverse process. Ridges on the cage side walls were designed to separate five pairs of material plates to create five bone conduction channels. These channels were open to both the underlying bone and overlying soft tissues (Fig. 1), had cross sections of 0.8×5.0 mm and were 8.0 mm in length. The polyacetal components were sterilized by soaking in 80% ethanol for at least 20 min and the metal screws were sterilized by autoclave.

2.3. Materials

Ceramic plates were manufactured to achieve ten conditions through a combination of ceramic composition, calcinations, sintering temperature and surface roughness, as specified in Table 1. Hydroxyapatite powder (HA, Merck, Germany), beta-tricalcium phosphate powder (TCP, Merck, Germany) and BCP powder (HA/TCP, weight% 80/20, IsoTis SA) were obtained commercially. A portion of HA powder was calcined by heating from ambient to 900 °C at a rate of 100 °C/h and then cooling naturally with no dwell period. Aqueous slurries of calcined HA, raw HA, raw TCP and raw BCP powders were prepared by the slow admixing of components. The calcined HA slurry consisted of 67.1 wt% calcined HA powder, 28.6 wt% demineralized water, 2.6 wt% ammonia solution (25%, Merck), 1.5 wt% deflocculant (Dolapix, Aschimmer & Schwarz GmbH, Germany), and 0.15 wt% of binder (CMC, Pomosin BV, The Netherlands) added once a homogenous blend was obtained. The raw HA, TCP and BCP slurries consisted of 56.4 wt% ceramic powder, 37.6 wt% demineralized water, 3.9 wt% ammonia solution and 2.1 wt% deflocculant. No binder was added to the raw powder slurries. Cubes of approximately $12 \times 12 \times 12$ mm were cast from these slurries and allowed to air dry for 12 h at ambient temperature followed by 24 h in an air-filled oven at 50 °C. Debinding of the

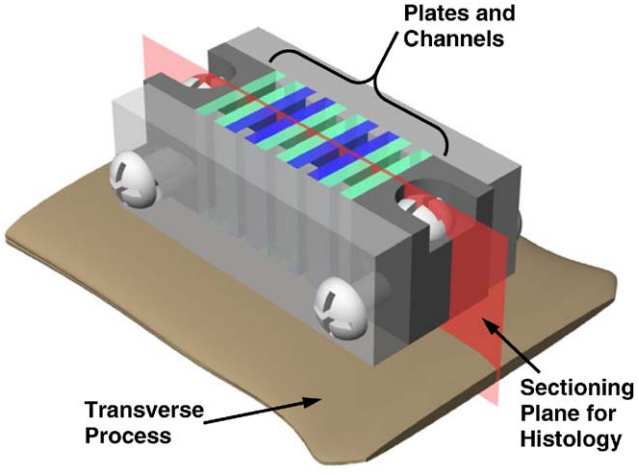

Fig. 1. Computer-generated image of conduction cage placed on a transverse process. The sectioning plane used for histology is indicated.

Table 1
Material conditions by calcination temp., sintering temp. and surface roughness

Ceramic material				Calcination temp.	Sintering temp.	Surface
BCP	r	h	r	n/a (raw)	1300 °C (high)	Rough
BCP	r	h	s	n/a (raw)	1300 °C (high)	Smooth
BCP	r	m	s	n/a (raw)	1200 °C (med)	Smooth
BCP	r	l	r	n/a (raw)	1150 °C (low)	Rough
BCP	r	l	s	n/a (raw)	1150 °C (low)	Smooth
TCP	r	l	s	n/a (raw)	1150 °C (low)	Smooth
HA	l	h	s	900 °C (low)	1250 °C (high)	Smooth
HA	l	l	s	900 °C (low)	1150 °C (low)	Smooth
HA	r	h	s	n/a (raw)	1250 °C (high)	Smooth
HA	r	l	s	n/a (raw)	1150 °C (low)	Smooth

ceramics was performed by heating at a rate of 0.5 °C/min to 400 °C and then cooling naturally with no dwell period. The ceramic cubes were then sintered using a 600 min heating phase and a 480 min dwell period at the appropriate sintering temperature (table 1) followed by natural cooling. Plates with dimensions of 7.0 mm × 8.0 mm × 1.1 mm were cut from sintered blocks using a sawing microtome (Leica, Germany). All plates were polished to 0.95 ± 0.03 mm in thickness using a rotary polisher and 1200 grit silicon carbide paper (Struers, Denmark) ensuring both sides of the plate were polished. Rough surfaces were created by unidirectionally abrading both sides of the plates on 120 grit paper. The plates were cleaned by ultrasound for 15 min each in acetone, 100% ethanol and demineralized water. After air drying at 50 °C, the scaffolds were sterilized by autoclave. Verification of the composition and phase purity of the plates was performed by FTIR and XRD analysis. Characterization of surface features and microporosity was conducted via scanning electron microscope (SEM) observation.

2.4. Implantation and fluorochrome labelling

Following the approval of the institutional animal care committee, ten adult female Dutch milk goats, aged 24–36 months, were acquired and allowed to acclimate for at least 4 weeks. Prior to the surgical procedure, two spinal cages for each animal were aseptically assembled with the ten material conditions arranged according to a randomized complete block design. The surgical procedures were performed under general inhalation anesthesia of a halothane gas mixture (Sanofi, The Netherlands) preceded by detomidine sedation (Pfizer, The Netherlands). After shaving and disinfecting the thoracolumbar region, a central skin incision, from approximately T8 to L5, was made to expose the muscle fascia. This incision supported implantation of the spinal implants as well as intramuscular and iliac implants that are not discussed in the present manuscript. Bilateral muscle incisions were then made and retracted to expose both transverse processes of the L4 vertebrae. The processes were decorticated using an angled bone rasp. Care was taken to ensure the even decortication of a flat surface with an area sufficient for placement of a cage. One cage was placed on each transverse process and pilot holes were drilled under saline irrigation. Two stainless steel self-tapping screws were then inserted to firmly attach each cage. Light finger pressure was applied to the top of each cage just prior to muscle closure to ensure the ceramic plates were in contact with the underlying bone. The muscle fascia was closed with non-resorbable sutures and the skin closed in two layers with resorbable sutures. Buprenorphin (Shering-Plough, The Netherlands) was administered for postoperative pain relief. Sequential fluorochrome markers were administered at 3, 5 and 7 weeks after implantation. Calcein Green (10 mg/kg intravenously, Sigma, The Netherlands) was administered at either 3 or 7 weeks, Xylenol Orange (80 mg/kg intravenously, Sigma, The Netherlands) was correspondingly administered at either 7 or 3 weeks and Oxytetracyclin (Engemycine 32 mg/kg intramuscularly, Mycofarm, The Netherlands) was always administered at 5 weeks. At 9 weeks, the animals were sacrificed by an overdose of pentobarbital (Organon, The Netherlands) and the implants retrieved.

2.5. Histological processing and histomorphometry

The explanted samples were fixed in a solution of 4% glutaraldehyde and 5% paraformaldehyde. Fixed samples were dehydrated by ethanol series and embedded in polymethylmethacrylate. Two centrally located (Fig. 1) 10 μm thick sections were cut from each sample using a sawing microtome (Leica, Germany). The first section remained unstained for epifluorescence microscopy and the second section was stained with methylene blue and basic fuchsin for routine histology. The general tissue response, bone formation and fluorochrome markers were evaluated using a light/fluorescence microscope (E600, Nikon, Japan) equipped with a quadruple filter block (XF57, dichroic mirror 400, 485, 558 and 640 nm, Omega Optics, The Netherlands). High resolution, low magnification (4 ×), digital fluorescent micrographs were made of unstained sections for histomorphometry. High-resolution digital scans of the stained sections were made for histomorphometry using a photographic film scanner (Dimage Scan Elite 5400, Minolta, Japan). Histomorphometry was performed using a PC-based system with the KS400 software (version 3, Zeiss, Germany). A custom macro was developed to measure the height of bone in each channel (bone height), percentage of available space occupied by bone in each channel (bone area%) and the length of direct contact between bone and ceramic in each channel (contact length). Bone height was effectively measured at 3, 5, 7 and 9 weeks by measuring the maximum height of each fluorochrome marker in the fluorescence images and the maximum bone height on the digital images of the stained sections.

2.6. Statistics

Box plots were used to display statistics of the measured parameters. To review, a box plot displays the lower, median and upper quartiles as well as the minimum and maximum of a data set. The box depicts the interquartile range and encompasses the middle 50% of the data values. The whiskers extend from the box to the minimum and maximum values. Observation between 1.5 and 3 times the interquartile range are outliers and observations greater than 3 times the interquartile range are extreme outliers. The data were

subsequently analyzed by ANOVA for randomized complete block design with a post hoc Tukey's HSD ($\alpha = 0.05$) to determine differences between material conditions. Partial correlation coefficients between measured parameters (9 weeks bone height, bone area% and contact length) were also calculated.

3. Results

3.1. Materials

The XRD patterns and FTIR spectra of the ceramic materials were indicative of the expected materials and demonstrated no extraneous phase impurities. As expected, lower sintering temperatures resulted in more amorphous materials, as demonstrated by broader peaks in the XRD patterns. Conversely, higher sintering temperatures resulted in more crystalline materials. No influence as a result of powder pre-calcinations was noted in the XRD patterns and FTIR spectra of the HA materials. SEM observations of the surface characteristics of the ceramic plates revealed general differences that correlated with material and sintering temperature (Fig. 2). The low- and medium-sintering temperature BCP materials exhibited a spectrum of surface micro- and macroporosity features from approximately 1–20 μm in size. In comparison, the high sintering temperature BCP materials displayed much less surface porosity features. The effect of the surface roughening procedure on the low and high sintering temperature BCP materials is apparent at lower magnifications (100 ×). The roughing resulted in wide gouges with a deep appearance for the low sintering temperature BCP while the high sintering temperature BCP exhibited relatively narrow and shallow scratches. At higher magnification (1000 ×), little difference was apparent between the rough and smooth surfaces for low sintering temperature BCP. However, the roughened high-temperature BCP material demonstrated a generally coarse surface texture as compared to the smooth high-temperature BCP. The surface features of the low sintering temperature HA materials did not appear to be influenced by the calcination treatment and displayed much more uniform surface microporosity, approximately 0.5–2 μm in size, in relation to the low-temperature BCP materials. At the higher sintering temperature the HA material exhibited much smoother surfaces with little microporosity, however, the calcination treatment appeared to increase the surface microporosity and texture somewhat. The TCP material, in contrast to the other materials sintered at low temperatures, exhibited very different surface microfeatures with intermixing patches of microporosity and smooth surfaces in near equal proportions.

3.2. In vivo results

There were no surgical complications and all cages were attached firmly to the underlying transverse process at retrieval. No macroscopic or microscopic indications of infection were found.

Histological observations of stained sections clearly revealed greater bone formation in low and medium sintering temperature materials compared to high sintering temperature materials with regard to bone area. Additionally, these materials demonstrated increased bone heights in the channels and displayed numerous sites of direct contact between bone and ceramic. In contrast, high sintering temperature BCP and HA materials had notably lower bone areas and heights in the channels with virtually no contact between bone and ceramic (Fig. 3). Although the amount of bone formation in the TCP channels was similar to that of the low sintering temperature BCP and HA materials, the trabecular like structures appeared thicker in comparison, particularly in close proximity to the transverse process. Also noteworthy was the visible degradation of the TCP material, particularly toward the channel end furthest from the transverse process. Precalcination of the HA powder and roughening of BCP surfaces demonstrated no observable influence compared to corresponding material and sintering conditions. Finally, the appearance of the ceramic materials themselves in the stained histological sections was noticeably different. In general, low sintering temperature materials appeared much darker compared to the lighter gray of the high sintering temperature materials (Fig. 3). The exception was the TCP material, which had a distinctly lighter appearance compared to the other low sintering temperature materials.

Epifluorescent microscopy of the sequential fluorochrome labels revealed the dynamics of bone formation in the channels (Fig. 4). All three labels were present in the healing bone of the transverse process. However, the first label (3 weeks) was not always present within the bone in the ceramic channels. The second (5 weeks) and third (7 weeks) labels were always present within bone in the channels. The fluorochrome labels indicated that the bone formation occurred in two manners, as a spur from the underlying transverse process or via nucleation of bone formation at distinct sites on the ceramic surface. The spur type bone formation had a centrally located early label (3 or 5 weeks) that did not connect with the ceramic surface within a channel. This early bone formation was then at least partially surrounded by a layer of bone containing a later label, which may or may not contact the ceramic surface. This was the primary mode of bone formation in the high sintering temperature HA materials. The nucleation-type bone formation presented as distinct sites where an early label was directly apposed or very near the ceramic surface. The

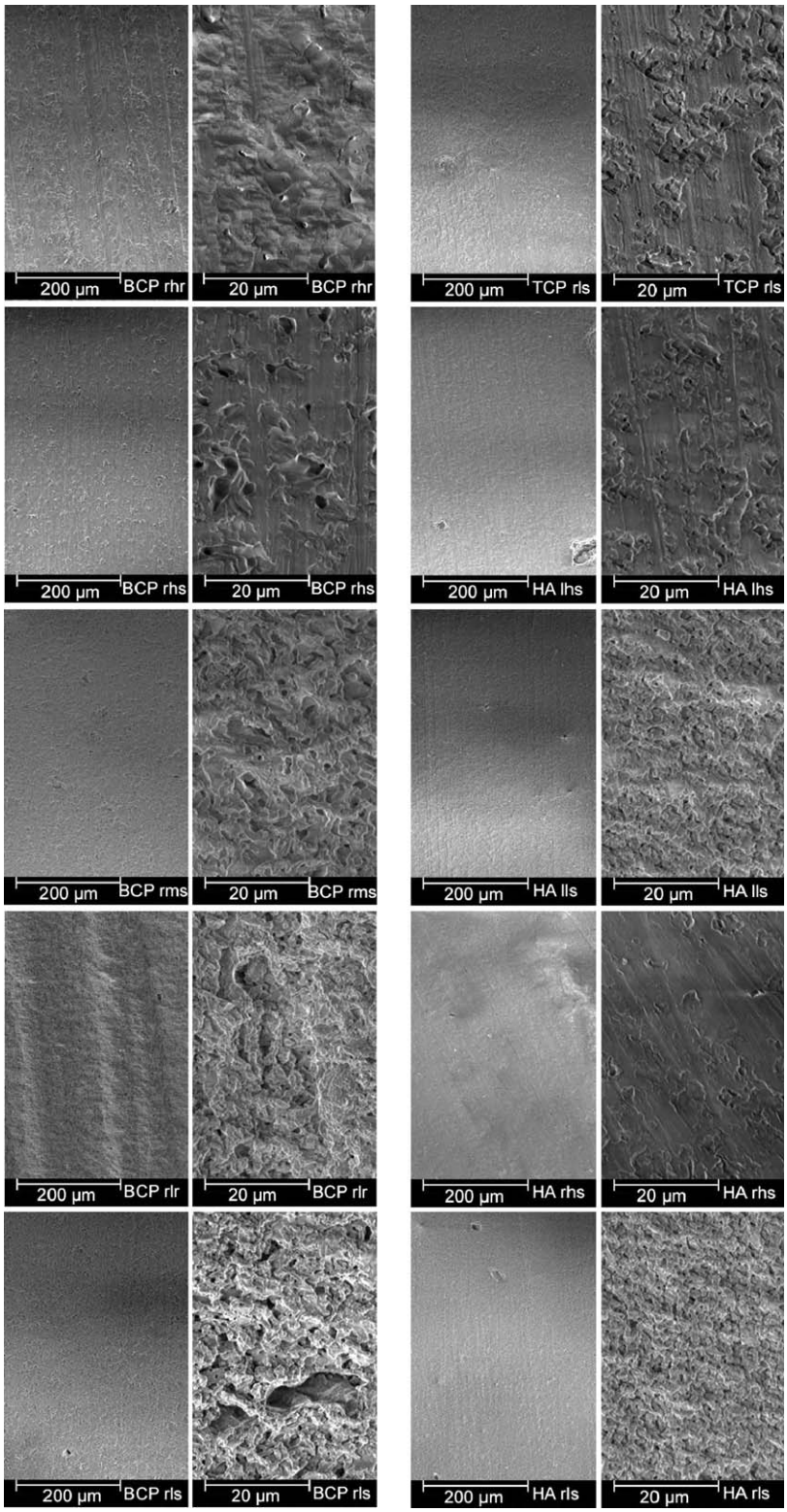

Fig. 2. Low and high magnification SEM micrographs of each of the ceramic materials used in this study. Material name and magnification are indicated in data bar at the bottom of each image. BCP materials are in left hand columns going from high sintering temperature (top) to low sintering temperature (bottom). Similarly, TCP and HA materials are in the right hand columns. Refer to Table 1 for specific material condition associated with material name.

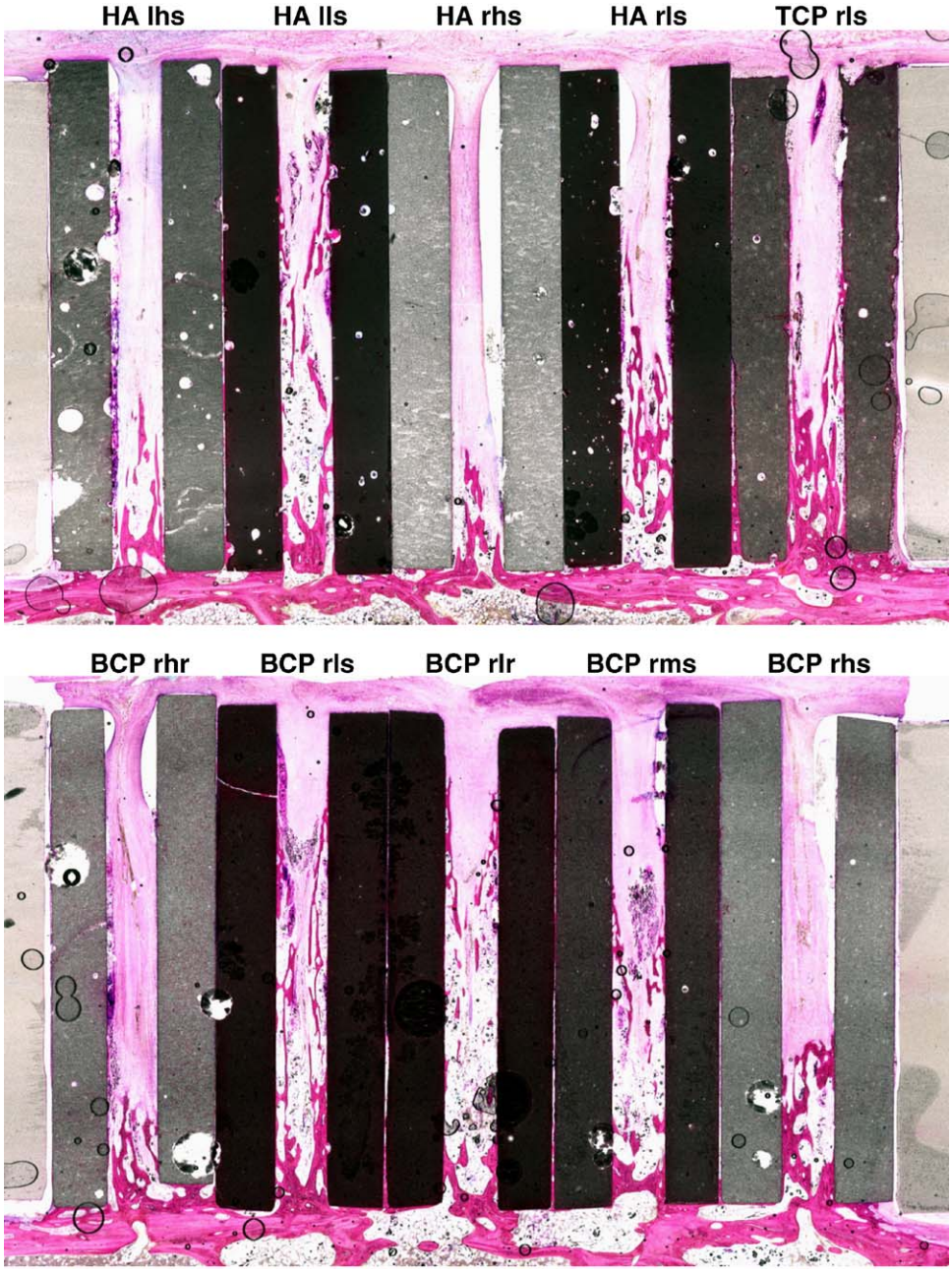

Fig. 3. Stained (methylene blue/basic fuchsine) histological sections. Bone is stained pink/red and the ceramic plates light to dark gray. The transverse process is at the bottom of the images and the polymer cage is visible at the extreme right and left of the images. Material treatment label (refer Table 1) is indicated above the conduction channels created by pairs of material plates.

order of fluorochrome labels then indicated that bone formation started at the surface and progressed toward the channel interior. Although these surface bone nucleation sites were often not connected by bone lying on the ceramic surface they were almost always connected by thin, trabecular like struts of bone lying away from the ceramic surface in the channel interior. This type of bone morphology was seen in the stained histology (Fig. 3). The nucleation type of bone formation was most prominent in the low and medium sintering temperature materials and was the exclusive means of bone formation at distances of more than a few millimeters from the transverse processes.

Histomorphometric data were analyzed graphically and statistically. Box plots of bone height at 3, 5, 7 and 9 weeks, shown in Fig. 5, demonstrate the progression of bone formation for the different material conditions. At 3 weeks, the high sintering temperature BCP materials (BCP rhr, BCP rhs) and, in particular, the high sintering temperature HA materials (HA lhs, HA rhs) exhibited inferior bone height compared to the six lower sintering temperature materials (BCP rms, BCP rlr, BCP rls, TCP

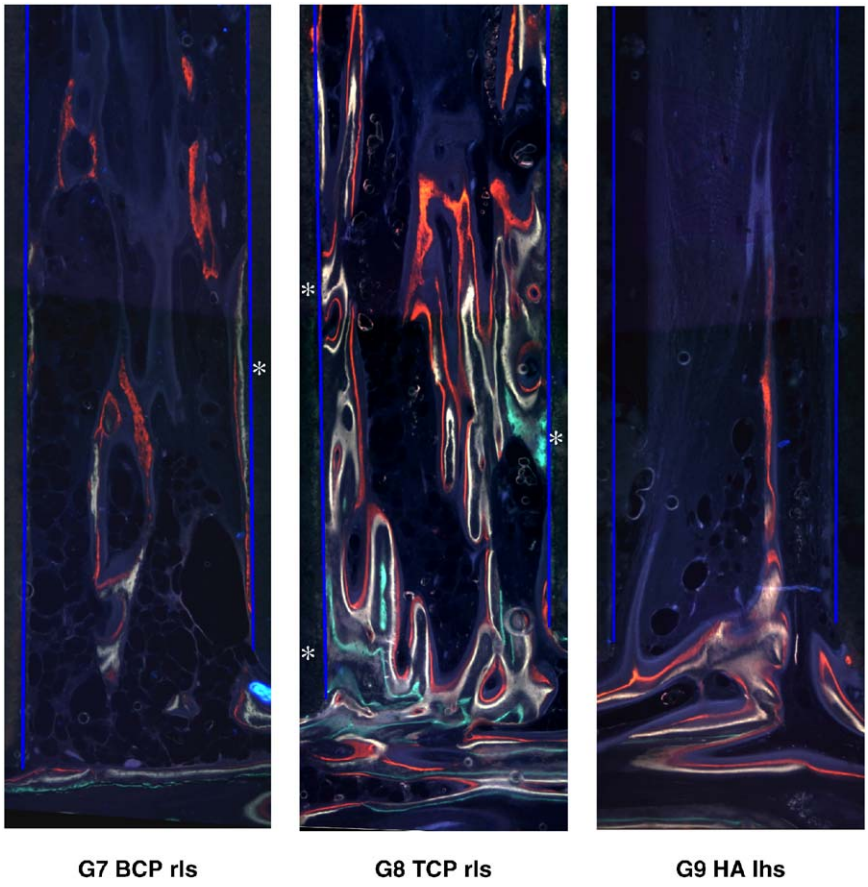

Fig. 4. Epifluorescent microscopy images of fluorochrome markers. Label at bottom of each image indicates the goat number and material treatment. In all three images the earliest label is green (3 weeks, calcein green), the middle label is yellow (5 weeks, oxytetracyclin) and the final label is orange (7 weeks, xylenol orange). Vertical blue lines indicate the approximate location of the ceramic surface. Examples of bonding osteogenesis are indicated by an *.

rls, HA lls and HA rls). All materials exhibited progressively greater bone height in the channels as the implantation period increased. However, the six lower sinter temperature materials continued to outperform the higher sintering temperature materials. Comparing 9 weeks bone height results with contact length and bone area%, a common pattern is apparent (see also Fig. 6). The two low-temperature BCP ceramics (BCP rls and BCP rlr), the medium temperature BCP ceramic (BCP rms) and the TCP ceramic (TCP rls) yield the highest mean values for all measurements. This is followed by the two low-temperature HA materials (HA lls and HA rls), then the two high-temperature BCP materials (BCP rhs and BCP rhr) and, finally, the two high-temperature HA materials (HA lhs and HA rhs). Statistical analyses were performed on the bone height, contact length and bone area% measurements at the end point of the 9 weeks implantation period, and demonstrated highly significant ($p<0.01$) differences within all three parameters. Post hoc, pairwise comparisons using Tukey's HSD test were performed to illustrate the significant differences between the ten material treatments for the three measurements. Fig. 7 graphically depicts these results. The material treatments in Fig. 7 have been generally ordered by their mean values and in the groupings suggested by the box plots. The same sequence is used for the three parameters to enable easier comparison of the significance patterns. Although the results are actually mirrored around the diagonal, displaying only the results above the diagonal enables the charts to be interpreted in a rowwise manner. In this case, when significance is indicated by a shaded block at the intersection of a row and column, the value for the material treatment represented by the row is *always significantly greater than* the value for the material treatment represented by the column. In general, there is a notable similarity between the significance patterns for the three parameters with material type and sintering temperature being the primary reasons for significant differences. Calcination of the HA powder consistently resulted in higher measurement means compared to the non-calcined (raw powder) ceramics with the same final sintering temperature (HA lls and HA rls, HA lhs and HA rhs). Additionally, the combination of pre-calcination with low sintering temperature yielded significantly higher values for all three measurements than both of

the high sintering temperature HA materials. However, the use of raw powder with a low sintering temperature did not demonstrate these significances. Roughening of the low and high temperature BCP surfaces had little influence compared to smooth surfaces. Finally, a partial correlation test between measured parameters was performed while controlling for material condition and revealed highly significant correlations ($p<0.01$) between all three measured parameters.

4. Discussion

We demonstrated in the current manuscript a new screening model that concerns early bone formation from the decorticated transverse process of the goat lumbar spine. The observed bone formation occurred by two modes depending upon the material treatment and manifested as either a spur extending from the underlying transverse process or via nucleation of bone

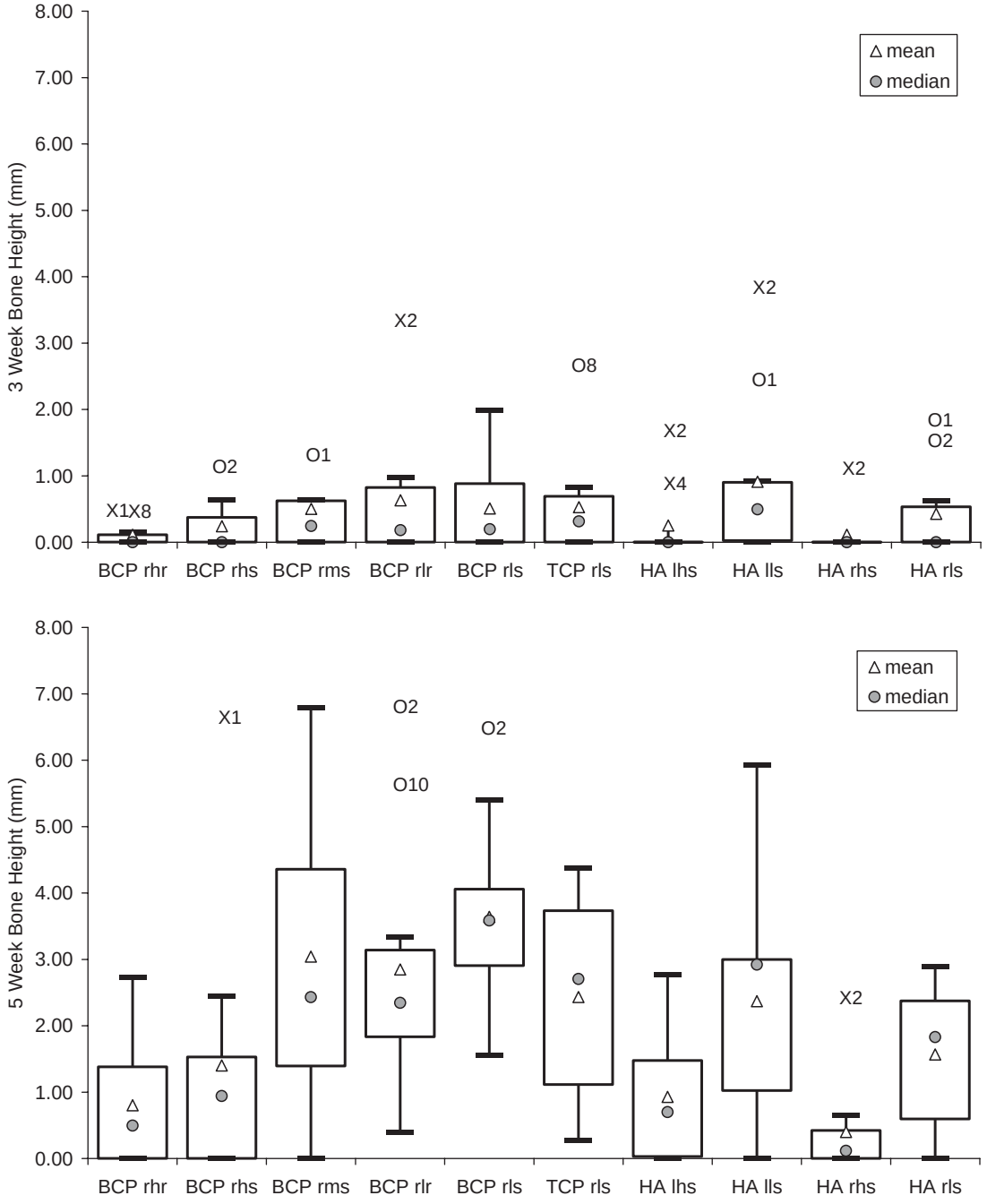

Fig. 5. Box plots of bone height at 3, 5 and 7 weeks, measured on fluorescent images, and at 9 weeks, measured on stained histology. The symbol "O" indicates and outlier and the symbol "X" indicates an extreme outlier. The number following these symbols indicates the animal associated with the measurement.

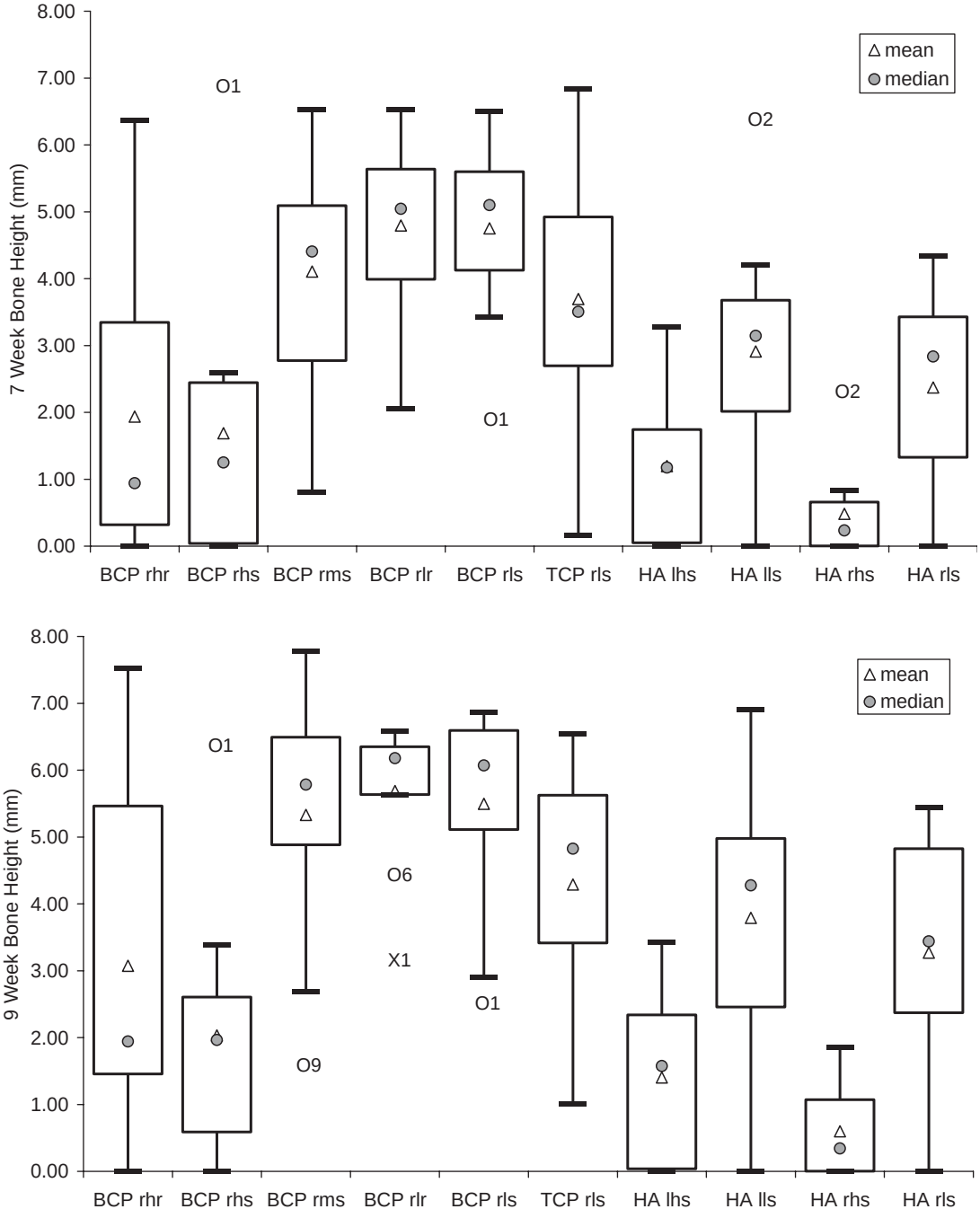

Fig. 5. (*Continued*)

formation at distinct sites on the ceramic surface. The spur-type bone formation was not dependent upon the surface of an implant. This type of bone formation has been labeled as bone ingrowth. In this study, bone ingrowth occurred in all materials but was the dominate mode of bone formation in the high sintering temperature ceramics, particularly the HA materials. The nucleation type bone formation was the dominant mode of bone formation in the lower sintering temperature ceramics and was observed to be highly surface dependant. This is termed osteoconduction and is described as the growth or spreading of bone over a surface. However, bone matrix does not have the intrinsic ability to grow or spread once formed. Therefore, it is a population of migratory osteogenic cells that are conducted along a surface and must be responsible for the bone formation. Once these cells begin producing matrix, they stop migrating [19]. Thus, osteoconduction may be defined as the spreading of bone over a surface preceded by the ordered migration of differentiating

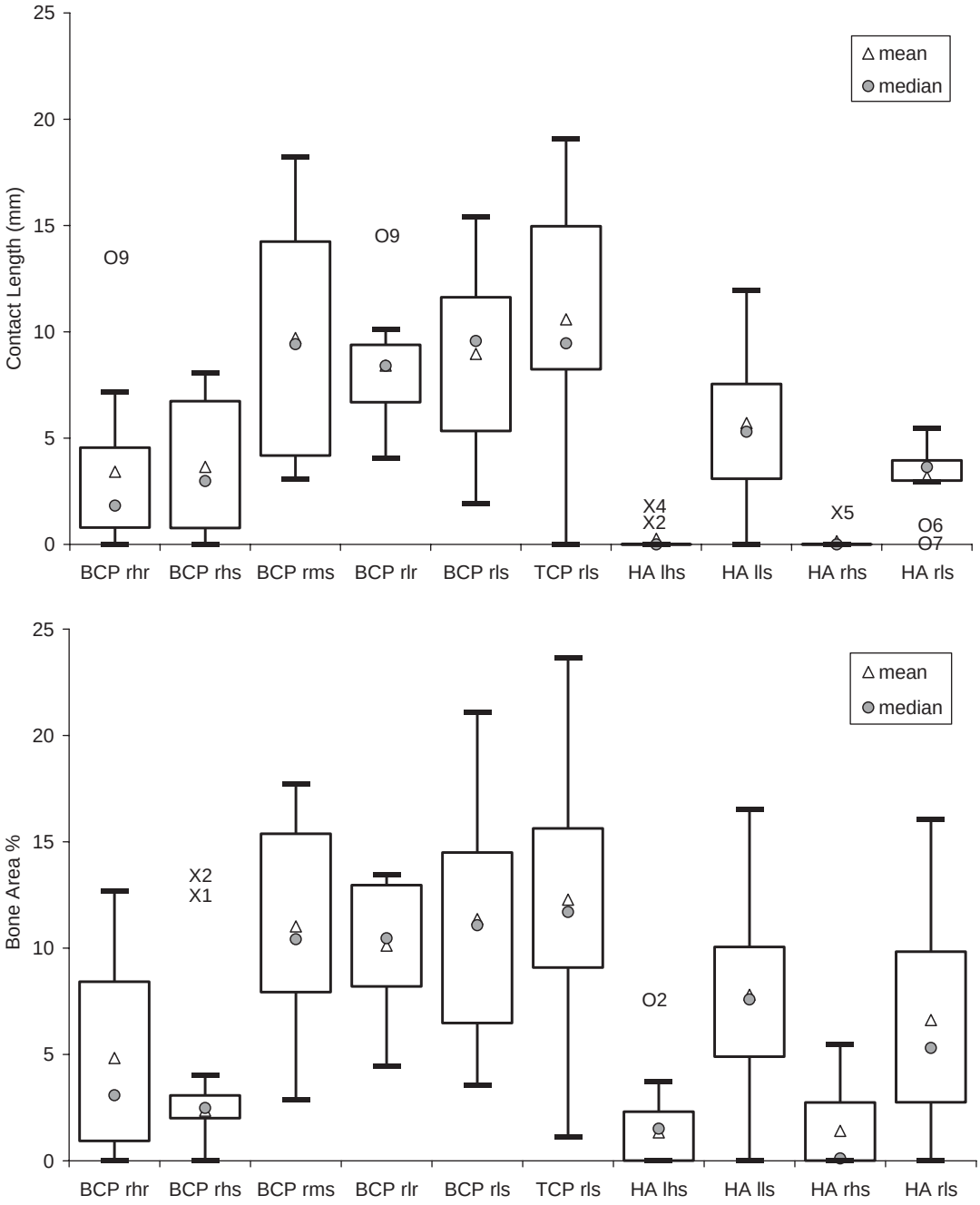

Fig. 6. Box plots of bone contact length and bone area% measured on stained histology. The symbol "O" indicates and outlier and the symbol "X" indicates an extreme outlier. The number following these symbols indicates the animal associated with the measurement.

osteogenic cells. An important aspect of osteoconduction is the direct bonding of bone matrix with the material surface without an interposing fibrous tissue layer, so-called bonding osteogenesis [20].

Materials that elicit a bonding osteogenesis response are termed bioactive. The bioactive process for ceramic materials has been covered in detail elsewhere [21–24] and is described by several basic steps: (1) the partial dissolution of the ceramic resulting in an increase in calcium and phosphate concentration in the local microenvironment; (2) precipitation of a carbonate calcium phosphate layer; (3) association and then incorporation of the precipitated layer with the organic matrix of newly formed bone. The formation of the prerequisite carbonate calcium phosphate layer is dependent upon the solubility or resorbability of the ceramic substratum. For example, BCP ceramics become more resorbable and exhibit a greater abundance of precipitated carbonate calcium phosphate when the ratio of β-TCP to HA is increased [25,26]. Sintering also

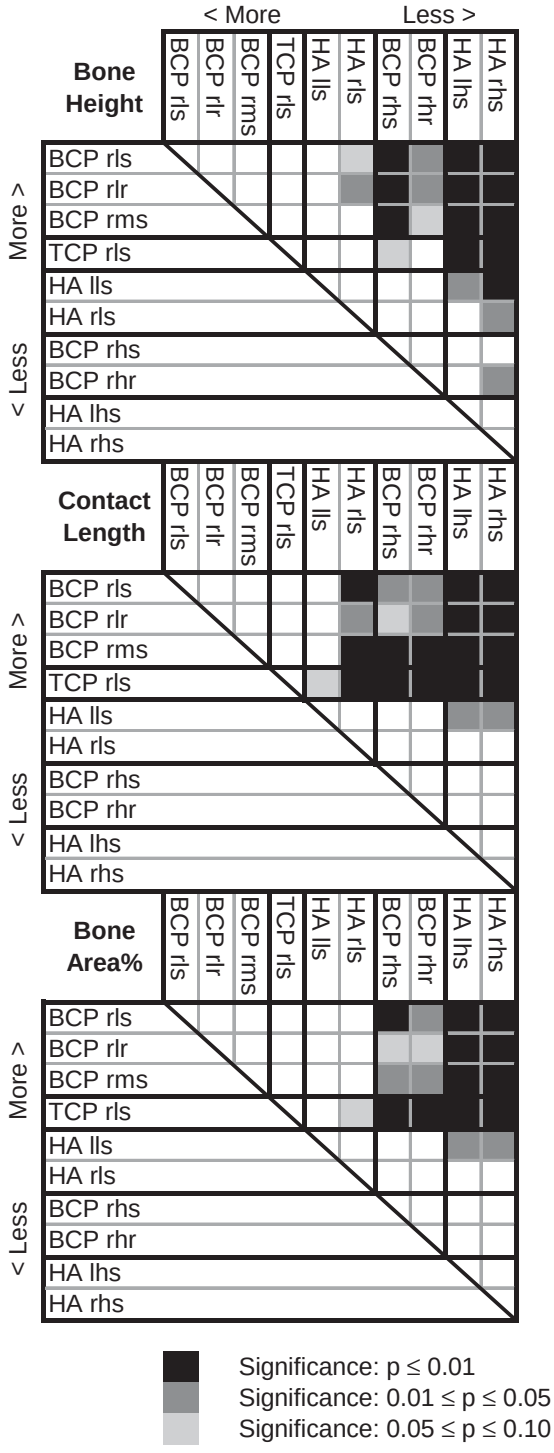

Fig. 7. Graphical representation of Tukey's HSD post hoc test to determine significant differences between material treatments. These charts are interpreted in a rowwise manner. When a shaded area lies at the intersection of a row and column, the material treatment represented by the row has a significantly higher mean than the material represented by the column. The legend at the bottom indicates the significance levels associated with the three shades of gray.

influences solubility with higher temperatures decreasing the solubility. This imparts a more detailed solubility range to the BCP and HA materials as a result of the sintering temperatures used in their production. Furthermore, microporosity has also been suggested as an important factor in the bioactivity of ceramics [27,28]. Microporosity can greatly increase the surface area of a ceramic, facilitating greater dissolution and, therefore, enhancing the precipitation of the carbonate calcium phosphate layer. Additionally, microporosity may enable bone morphogenic proteins adsorbed on their surface to reach local concentrations greater than the threshold value needed to induce bone formation [14,25,28]. Microporous surfaces may also enhance the adhesion, proliferation, differentiation and matrix deposition of osteogenic cells [29,30].

Although dissolution characteristics were not assessed in this study, well-established data regarding the dissolution characteristics of calcium phosphate materials [31,32] may be used to order the expected solubility of the ceramics in this study. The overall dissolution characteristics result from the interaction of material chemistry, sintering temperature and microporosity. The solubility order based on chemistry alone is: TCP $\gg$ BCP $>$ HA. It is important to note that the BCP material in this study is approximately 80% HA. Therefore, based on chemistry alone, the BCP is likely to behave more similarly to HA than to TCP. Considering sintering temperature, the solubility of the BCP and HA materials can be ordered as follows: BCP (low) $>$ BCP (medium) $>$ BCP (high) and HA (low) $>$ HA (high). Higher sintering temperatures increase the crystallinity (reduce vacancies in crystal lattice) and increase crystal grain size, both of which reduce solubility. Finally, the ceramics can be ordered based on the amount of surface microporosity as determined by SEM observation: BCP (low sintering temp.) $>$ BCP (medium sintering temp.) $>$ HA (low sintering temp.) $>$ TCP $>$ BCP (high sintering temp.) $>$ HA (high sintering temp.). Microporosity was generally associated with lower sintering temperatures. However, microporosity can only modulate the solubility of a material by changing the surface area. Therefore, the solubility of materials used in this study will be in line with the predictions made from chemistry and sintering temperature with microporosity increasing the solubility of the lower sintering temperature materials. We can predict the following solubility order with some certainty: TCP $>$ BCP (low) $>$ BCP (medium) $>$ BCP (high) $>$ HA (high). The low sintering temperature HA cannot be precisely placed in this order, however, we know that it will be less soluble than BCP (low) and more soluble than HA (high).

While all the materials in this study have been previously described as bioactive [33–36] and did exhibit areas of direct bone bonding, observations and measures of this activity varied with material conditions. These variations in bioactivity agreed very well with the literature cited in the previous paragraphs. As a rule,

the bioactivity, as determined by observation and histomorphometry, correlated accurately with the expected solubility of the ceramics. Low and medium sintering temperature BCP materials (BCP rls, BCP rlr and BCP rms) and the single TCP material (TCP rls) yielded similar but significantly higher values for bone height (9 weeks), contact length and bone area% compared to HA and, in most cases, BCP materials sintered at high temperatures (HA lhs, HA rhs, BCP rhs and BCP rhr). The low sintering temperature HA materials (HA lls and HA rls), while not achieving the same mean values as TCP and the low and medium temperature BCP materials, attained greater values than the high-temperature materials.

Several specific observations from the current study are of particular interest. First, osteoconductive and bioactive qualities were virtually absent from the high sintering temperature materials. Second, TCP, despite noticeably less surface microporosity, performed as well as the low and medium sintering temperature BCP materials (TCP was also sintered at low temperature). This suggests that microporosity may not play as critical a role in bioactivity as suggested by others [28–30], and that another property of the material, such as solubility, is more essential. TCP was certainly the most soluble material in the current study as it was the only material with observable degradation. Third, the bioactivity of low sintering temperature HA materials was improved by using calcined HA powder as compared to raw HA powder. The reason for this is not clear, however, it is known that calcination treatment provides a more spherical powder morphology [37]. This may result in a more interconnected microporosity in the ceramic plates made from calcined powder as compared to raw powder. This, in turn, would enhance the solubility characteristics of this material and the subsequent precipitation of a carbonate calcium phosphate layer. Finally, the surface roughness imparted on the low and high sintering temperature BCP materials had no observed or measured influence on bone formation. The high magnification SEM observations indicate a likely reason for this. The roughening protocol used in this study did not appreciably impact the surface roughness at the microscale and therefore did not appreciably alter any material parameters related to bioactivity.

It is difficult to ignore the similarity, both in appearance and definition, between osteoconduction and osteoinduction [13,38]. Urist defined osteoinduction as the mechanism of cellular differentiation towards bone of one tissue due to the physiochemical effect of contact with another tissue [39]. At the time, only tissues, such as demineralized bone matrix and uroepithelium, were known to have this ability. More recently, some synthetic biomaterials have also been recognized as osteoinductive, i.e. they can induce bone formation at extraskeletal locations [28,40,41]. Bone formation in both osteoconduction and osteoinduction relies upon differentiated bone cells producing bone matrix which is then mineralized. The critical difference between the phenomena is the population of cells involved. Osteoconduction can draw upon a population of osteoprogenitor cells in adjacent bone tissue. Osteoinduction relies upon a population of cells available either in the local tissue (e.g. muscle or subcutaneous tissue) or systemically. Despite this difference, the mechanisms involved are likely to be very similar and insights into these mechanisms will be beneficial to understanding both phenomena.

The new model presented in this paper provides an efficient means of screening the influence of parameters on the process of early bone formation in a large animal and at a clinically relevant location. This model is easily applied and readily adaptable to the materials and treatments of interest. The model, as demonstrated in this manuscript, not only allows the performance of the materials/treatments to be gauged but may also enable the fundamental processes involved in bone formation to be studied.

5. Conclusions

The current study validates a new model for screening multiple material conditions that is clinically relevant for posterior spinal fusion. This model facilitates the use of completely randomized block designs and supporting statistics. Clearly demonstrated are the differences, both observed and measured, between ten calcium phosphate ceramics with regard to the initial process of bone formation from the goat transverse process.

Acknowledgments

The authors would like to thank The Netherlands Technology Foundation (STW, Grant UGN.4966) and the Anna Foundation for their financial support.

References

[1] Albee F. An experimental study on bone growth and the spinal bone transplant. J Am Med Assoc 1913;60:1044–52.
[2] Banwart JC, Asher MA, Hassanein RS. Iliac crest bone graft harvest donor site morbidity. A statistical evaluation. Spine 1995;20(9):1055–60.
[3] Younger EM, Chapman MW. Morbidity at bone graft donor sites. J Orthop Trauma 1989;3(3):192–5.
[4] Gazdag AR, Lane JM, Glaser D, Forster RA. Alternatives to autogenous bone graft: efficacy and indications. J Am Acad Orthop Surg 1995;3(1):1–8.
[5] Hollinger JO, Brekke J, Gruskin E, Lee D. Role of bone substitutes. Clin Orthop 1996;324:55–65.

[6] Jarcho M. Calcium phosphate ceramics as hard tissue prosthetics. Clin Orthop 1981;157:259–78.
[7] Bucholz RW. Nonallograft osteoconductive bone graft substitutes. Clin Orthop 2002;395:44–52.
[8] Ransford AO, Morley T, Edgar MA, Webb P, Passuti N, Chopin D, et al. Synthetic porous ceramic compared with autograft in scoliosis surgery. A prospective, randomized study of 341 patients. J Bone Jt Surg Br 1998;80(1):13–8.
[9] Le Huec JC, Lesprit E, Delavigne C, Clement D, Chauveaux D, Le Rebeller A. Tri-calcium phosphate ceramics and allografts as bone substitutes for spinal fusion in idiopathic scoliosis as bone substitutes for spinal fusion in idiopathic scoliosis: comparative clinical results at four years. Acta Orthop Belg 1997;63(3):202–11.
[10] Delecrin J, Takahashi S, Gouin F, Passuti N. A synthetic porous ceramic as a bone graft substitute in the surgical management of scoliosis: a prospective, randomized study. Spine 2000;25(5):563–9.
[11] Sandhu HS, Boden SD, An H, Kang J, Weinstein J. BMPs and gene therapy for spinal fusion: summary statement. Spine 2003;28(15, Suppl.):S85.
[12] Kruyt MC, Dhert WJ, Oner C, van Blitterswijk CA, Verbout AJ, de Bruijn JD, et al. Optimization of bone-tissue engineering in goats Bone tissue engineering and spinal fusion: the potential of hybrid constructs by combining osteoprogenitor cells and scaffolds. J Biomed Mater Res 2004;69B(2):113–20.
[13] Kruyt MC, van Gaalen SM, Oner FC, Verbout AJ, de Bruijn JD, Dhert WJ. Bone tissue engineering and spinal fusion: the potential of hybrid constructs by combining osteoprogenitor cells and scaffolds. Biomaterials 2004;25(9):1463–73.
[14] Ripamonti U. Osteoinduction in porous hydroxyapatite implanted in heterotopic sites of different animal models. Biomaterials 1996;17(1):31–5.
[15] Yuan H, Yang Z, De Bruij JD, De Groot K, Zhang X. Material-dependent bone induction by calcium phosphate ceramics: a 2.5-year study in dog. Biomaterials 2001;22(19):2617–23.
[16] Khan SN, Lane JM. Spinal fusion surgery: animal models for tissue-engineered bone constructs. Biomaterials 2004;25(9): 1475–85.
[17] Sandhu HS, Kanim LEA, Girardi F, Cammisa FP, Dawson EG. Animal models of spinal instability and spinal fusion. In: An YH, Friedman RJ, editors. Animal models in orthopaedic research. Boca Raton, FL: CRC Press; 1999. p. 505–26.
[18] Spivak JM, Ricci JL, Blumenthal NC, Alexander H. A new canine model to evaluate the biological response of intramedullary bone to implant materials and surfaces. J Biomed Mater Res 1990;24(9):1121–49.
[19] Davies JE, Hosseini MM. Histodynamics of endosseous wound healing. In: Davies JE, editor. Bone engineering. Toronto: EM Squared; 2000. p. 1–14.
[20] Davies JE. Mechanisms of endosseous integration. Int J Prosthodont 1998;11(5):391–401.
[21] Kokubo T, Kim HM, Kawashita M. Novel bioactive materials with different mechanical properties. Biomaterials 2003;24(13): 2161–75.
[22] Daculsi G. Biphasic calcium phosphate concept applied to artificial bone, implant coating and injectable bone substitute. Biomaterials 1998;19(16):1473–8.
[23] de Bruijn JD, Klein CP, de Groot K, van Blitterswijk CA. The ultrastructure of the bone-hydroxyapatite interface in vitro. J Biomed Mater Res 1992;26(10):1365–82.
[24] de Bruijn JD, van Blitterswijk CA, Davies JE. Initial bone matrix formation at the hydroxyapatite interface in vivo. J Biomed Mater Res 1995;29(1):89–99.
[25] Daculsi G, LeGeros RZ, Heughebaert M, Barbieux I. Formation of carbonate-apatite crystals after implantation of calcium phosphate ceramics. Calcif Tissue Int 1990;46(1):20–7.
[26] LeGeros RZ, LeGeros JP, Daculsi G, Kijkowska R. Calcium phosphate biomaterials: preparation, properties and biodegradation. In: Wise DL, editor. Encyclopedic handbook of biomaterials and bioengineering. Part A: Materials. New York: M. Dekker; 1995. p. 1429–63.
[27] Daculsi G, Bouler JM, LeGeros RZ. Adaptive crystal formation in normal and pathological calcifications in synthetic calcium phosphate and related biomaterials. Int Rev Cytol 1997;172: 129–91.
[28] Yuan H, Kurashina K, de Bruijn JD, Li Y, de Groot K, Zhang X. A preliminary study on osteoinduction of two kinds of calcium phosphate ceramics. Biomaterials 1999;20(19):1799–806.
[29] Kawai N, Niwa S, Sato M, Sato Y, Suwa Y, Ichihara I. Bone formation by cells from femurs cultured among three-dimensionally arranged hydroxyapatite granules. J Biomed Mater Res 1997;37(1):1–8.
[30] Lampin M, Warocquier C, Legris C, Degrange M, Sigot-Luizard MF. Correlation between substratum roughness and wettability, cell adhesion, and cell migration. J Biomed Mater Res 1997;36(1): 99–108.
[31] de Groot K. Degradable ceramics. In: Williams DF, editor. Biocompatibility of clinical implant materials. Boca Raton, FL, USA: CRC Press; 1981. p. 199–222.
[32] Elliott JC. Structure and chemistry of the apatites and other calcium orthophosphates. Amsterdam: Elsevier Science B.V.; 1994.
[33] de Groot K. Calcium phosphate ceramics: their current status. In: Boretos JW, Eden M, editors. Contemporary biomaterials. USA: Noyes Publications; 1984. p. 477–92.
[34] Ducheyne P. Bioactive ceramics. J Bone Jt Surg Br 1994;76(6): 861–2.
[35] Daculsi G, Passuti N. Bioactive ceramics, fundamental properties and clinical applications: the osseo-coalescence process. Bioceramics 1989;2:3–10.
[36] LeGeros RZ, LeGeros JP. Calcium phosphate biomaterials in medical applications. Bioceramics 1996;9:7–10.
[37] Patel N, Gibson IR, Ke S, Best SM, Bonfield W. Calcining influence on the powder properties of hydroxyapatite. J Mater Sci Mater Med 2001;12(2):181–8.
[38] Yang ZJ, Yuan H, Zou P, Tong W, Qu S, Zhang XD. Osteogenic responses to extraskeletally implanted synthetic porous calcium phosphate ceramics: an early stage histomorphological study in dogs. J Mater Sci Mater Med 1997;8(11):697–701.
[39] Urist MR, Silverman BF, Buring K, Dubuc FL, Rosenberg JM. The bone induction principle. Clin Orthop 1967;53:243–83.
[40] Ripamonti U. Bone induction in nonhuman primates. An experimental study on the baboon. Clin Orthop 1991;269: 284–94.
[41] de Bruijn JD, Yuan H, Dekker R, Layrolle P, de Groot K, van Blitterswijk CA. Osteoinductive biomimetic calcium phosphate coatings and their potential use as tissue engineering scaffolds. In: Davies JE, editor. Bone engineering. Totonto: EM Squared; 2000. p. 421–31.